Optimal Choice of the Number of Ground Control Points for Precise DSM Generation Using Light-Weight UAV in Small and Medium-Sized Open-Pit Mine

Nguyen Quoc Long[1, *], Ropesh Goyal[2], Luyen K. Bui[1],
Cao Xuan Cuong[1], Le Van Canh[1], Nguyen Quang Minh[1], Xuan-Nam Bui[3]

* Corresponding author: Nguyen Quoc Long, nguyenquoclong@humg.edu.vn

1. Hanoi University of Mining and Geology, 18 Vien street, Hanoi, 10000, Vietnam nguyenquoclong@humg.edu.vn; ORCID: 0000-0002-4792-3684
2. Indian Institute of Technology Kanpur, Kanpur-208016, Uttar Pradesh, India. ORCID: 0000-0002-2178-3265
3. Faculty of Mining Hanoi University of Mining and Geology, 18 Vien street, Hanoi, 10000, Vietnam, ORCID: 0000-0001-5953-4902

Abstract: UAV technology has been applied for DSM generation in open-pit mining of which the precision is improved by increasing the number of Ground Control Points (GCPs). However, DSMs are updated frequently in an open-pit mine where the surface is excavated continuously, making GCPs more challenged to be arranged in the field. An optimal number of GCPs should therefore be determined to select the locations of GCPs to reduce the risk of destroying them. This study investigates the influence of the numbers of GCPs and their network configuration in the Long Son quarry, Vietnam. The analysis involved DSMs generated from eight cases with a total of 18 GCPs, each has five configurations. The inter-case and intra-case accuracy of DSMs is assessed on $\mathrm{RMSE_{XY}}$, $\mathrm{RMSE_{Z}}$, and $\mathrm{RMSE_{XYZ}}$. The results show that, for a small- or medium-sized open-pit mine with an area of approximately 36 hectares, five GCPs are sufficient to achieve an overall accuracy of less than 10 cm. It is further shown that the optimal choice of the number of GCPs for DSM generation in such a mining site is seven due to a significant improvement in accuracy (<3.5 cm) and decrease in configuration dependency with respect to five GCPs.

KEY WORDS: Light-Weight UAV, Digital Surface Model, Ground Control Points, Small and Medium-Sized Open-pit Mine.

1. Introduction

Small and medium-sized open-pit mines such as quarries are often located in areas with complicated terrains and a variety of geological conditions. Many of them are high limestone mountains with significant changes in terrain elevation, while others are at a height of 100 m below the sea level. These lead to challenges for ground surveying using the traditional methods because of the limited accessibility in the mining area or even inaccessibility in some extreme cases.

The rapid development of Unmanned Aerial Vehicle (UAV) technologies has brought many benefits to the mining industry in terms of safety, precision, and productivity. Recently, UAVs have been used extensively in open-pit mining areas for numerous applications such as pit and dump management (Padró et al., 2019), stockpile management (Raeva et al., 2016), mapping of inaccessible steep inclines and cliffs (Fernández-Lozano et al., 2018), monitoring the dust particles (Alvarado et al., 2015), assessment of slope stability and mine subsidence (Ge et al., 2016), monitoring and analyzing subsurface heating (Malos et al., 2013), geological modelling (Szentpeteri et al., 2016) along with other applications involving assets and infrastructure management/inspections and as-built versus as-designed comparison. A detailed overview of the possible applications in the open-pit mining industry using different sensors attached to the UAVs is well documented in Ren et al. (2017).

Most of the applications mentioned above require a precise high-resolution DSM. There have been several studies on the generation of DSMs using UAVs for mining sites (e.g., Cryderman et al., 2014; Francioni et al., 2015; Shahbazi et al., 2015; Kršák et al., 2016; Szentpeteri et al., 2016; Bui et al., 2017; Esposito et al., 2017; Kovanič et al., 2017; Beretta et al., 2018; Forlani et al., 2018; Nguyen et al., 2019). Open-pit mining involves continuous excavation over time, and hence, surveying needs to be done at regular intervals. UAV-based surveying alone is not much advantageous until it is attached to precise ground control points (GCPs). This is because the in-built GNSS in low-cost and lightweight UAVs do not meet the accuracy requirement. Canh et al. (2020) have shown that with direct georeferencing of imagery data captured using light-weight UAV with onboard RTK positioning (DJI Phantom 4 RTK), it is not possible to obtain even the decimeter-level accurate DSM in complex mining terrains, such as ours. Some studies have also suggested the use of a few GCPs to achieve certain accuracy level as compared to GCP based geo-referencing or indirect geo-referencing, and more importantly, to prevent the biases in focal length within the self-camera-calibration technique (Mian et al., 2015; Hugenholtz et al., 2016; Gianfranco et al., 2018). However,

obtaining the vertical accuracy well within 5 cm with the direct georeferencing in light-weight UAVs is still challenging, especially for the open-pit mines. Thus, it becomes inevitable for indirect georeferencing of the collected UAV data sets using precise GCPs acquired using a dual-frequency GNSS receiver.

The accuracy achieved in the indirect georeferencing is dependent on the characteristics of GCPs, including the measurement precision and the distribution (i.e., the number of points and their spatial distribution) (James et al., 2017 a, b). It is a well-established fact that a higher number of uniformly distributed GCPs will reduce the errors in georeferencing, and thus increase the accuracy of the generated DSM (James et al., 2017b). However, one of the most important factors to introduce the UAV to the mining sector was to reduce the cost and increase the productivity and safety. This aims at choosing the optimal number of required GCPs, that is the minimal sufficient in number and also convenient to be organised in the field (their distribution), for our case an open-pit mine.

There have been several studies to analyse the effect of the number and distribution of GCPs to construct a precise DSM (e.g., Mancini et al., 2013; Tahar, 2013; Tonkin and Midgley, 2016; Agüera-Vega et al., 2017; Conveney and Roberts, 2017; Rangel et al., 2018). However, only a few studies have been applied to open-pit mines and relatively less for small to medium-sized open-pit mines. It becomes a challenging task, especially for small to medium-sized open-pit mines, because of the smaller site area and large undulations/depths. Shahbazi et al. (2015) analysed the number and distribution of GCPs for DSM generation in an open-pit mine using UAV. They conducted experiments with six different sets of which only one set consists of 22 GCPs and all the others have 3 GCPs. The authors recommended using a large number of well-distributed GCPs to achieve the highest precision. Villanueva and Blanco (2019) used four different distribution patterns of data sets that consist of 4, 6, 8, 12, 16, and 20 GCPs to analyse the effect of the number and distribution of GCPs for the stockpile measurement. No other study in the literature can be found by the authors discussing in detail the effect of the number and distribution of GCPs in DSM construction of small to medium-sized open-pit mines using light-weight UAVs.

In this paper, through rigorous experiments, we focus on delivering a detailed discussion on the optimal choice of the number of GCPs to achieve the most precise DSM in small to medium-sized open-pit mines. This is optimized in such a way that, given fewer GPSs are required, the locations of stable GCPs' monuments can be arranged more easily. This study is important because of the similar mining practiced in several

parts of the world, and extensively in Vietnam. The study focuses on the Long Son quarry that is of a typical configuration in its size, height difference, and surface roughness. Therefore, the results investigated from this study can be of assistance in designing networks of GCPs used for UAV-based topographical mapping in similar small- or medium-sized quarries in Vietnam.

2. Study area and materials

2.1. Study area

In this study, the experiments are conducted in the Long Son limestone quarry located in Thanh Hoa province in northern Vietnam, between latitudes 20°04′00″N and 20°05′30″N and longitudes 105°55′15″E and 105°56′00″E (Figure 1). The total area of this mine is approximate 1.0 km^2 with an exploitation reserve of 4.0 million tons per year. Like many other quarries in Vietnam, topographical characteristics of this quarry include benches, the toe of the benches, and steep slopes. At the time of the study, the mine was at the excavating level of 110 m. The maximum terrain difference is about 112 m, the average height of benches is 41 m, and the steepest slope is approximately 88 degree.

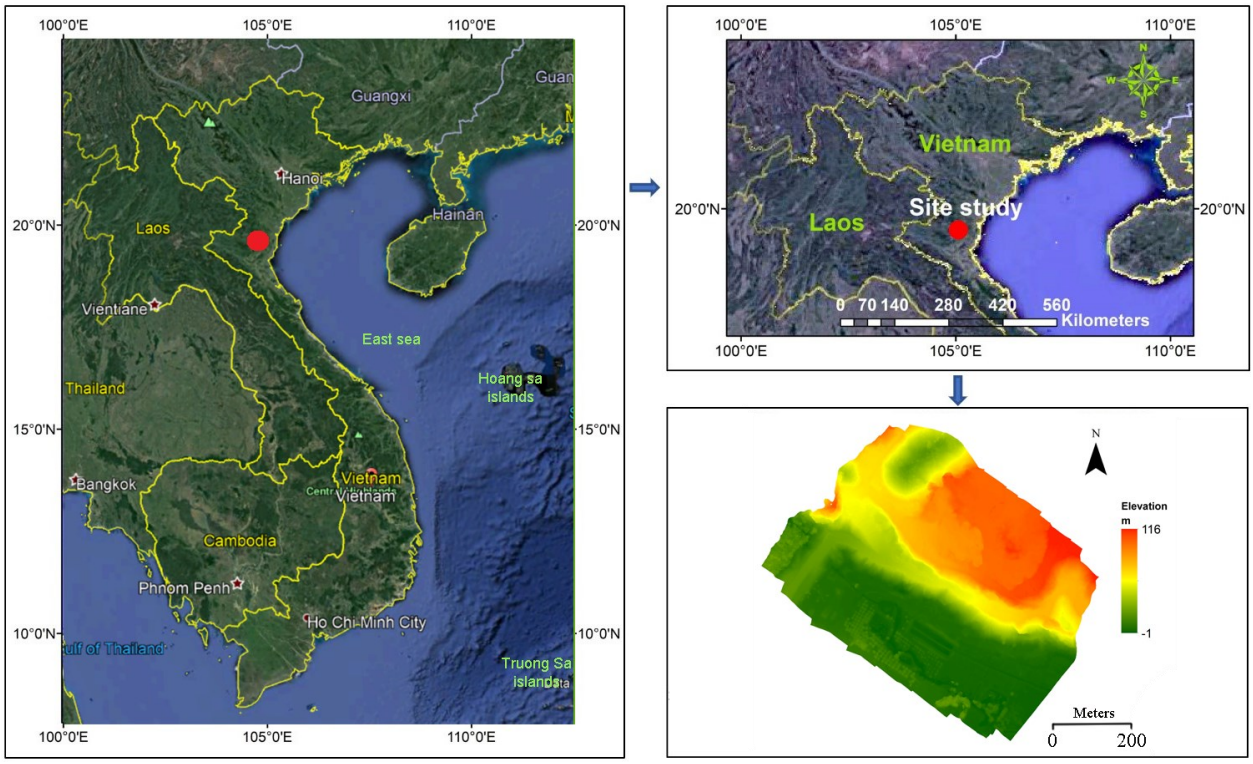

Figure 1. Location and Digital Elevation Model of the study site.

2.2. Data collection

For UAV survey, a DJI Phantom 4 Pro equipping with a 20-megapixel red, green, and blue camera and a GNSS/IMU is employed. The camera's focal length is 8.8 mm,

and the size of the sensor is 13.2 mm width by 8.8 mm height (https://www.dxomark.com). The UAV is a commercial light-weight quadcopter with manual or automatic flight modes set in Android or IOS smartphone applications. In this study, Pix4Dcapture installed on an iPhone 7 plus is used for flight planning. In the automatic mode, several important parameters are uploaded to the UAV, including a mapping area of 36 hectares, a flight height of 200 m above the ground, as well as image forward and side-overlap of 80%. Also, a GNSS/IMU mounted on the UAV allows positioning each camera with an average precision of 2.5 m. The positioning information of cameras is stored in each image's file and is used for processing imagery to obtain photogrammetric products. The imagery acquisition was completed with 80 photos and the ground sample distances (GSD) ranging between 4.66 and 7.58 cm/pixel.

Field reconnaissance is conducted using a handheld GPS (Mapinr v3.8 installed in a smartphone) to select relatively safe areas for establishing the 18 GCPs while maintaining a nearly uniform distribution. In order to easily detect the GCPs in the acquired images, they are marked with a 60 cm x 60 cm highly reflective material on the ground (Figure 2) for enhancing the contrast. The coordinates of the centre point of these GCPs are measured in the Vietnam national control network (the VN2000 coordinate system) using the GNSS/RTK method. The base receiver is installed at one control point of the national control network established in the local area. The CHC X91B receivers produced by CHCNAV were used for GNSS measurement. The specification of these receivers is shown in Table 1.

Figure 2. GCP marks and their coordinates measured by GNSS/RTK.

Table 1. The specifications of CHC X91B.

CHC X91 GNSS Receiver

	Signal	GPS: L1, L2, L5; GLONASS: L1, L2; BDS: B1, B2, B3; SBAS: WAAS, EGNOS, MSAS
	Kinematic	
	Horizontal:	+ (10mm + 1ppm) RMS
	Vertical:	+ (20mm + 1ppm) RMS
	Static	
	Horizontal:	+ (5mm + 1ppm) RMS
	Vertical:	+(10mm + 1ppm) RMS

3. Methodology

3.1. Experiment organisation

To analyse the effect of the number of GCPs and their distribution on the accuracy of a DSM, we test with five different configurations of eight sets of GCP networks, i.e., a total of 40 DSMs are generated. The eight sets of 18 GCPs include networks of 3-15, 4-14, 5-13, 6-12, 7-11, 8-10, 15-3, and 16-2 points, in which the first number represents the number of GCPs used for calibration of the camera-lens model and the second number represents the total number of GCPs used for the assessment of the constructed DSM. The five different configurations for each of the eight cases are depicted in Section 4 (see Table 4 and Table 5).

3.2. Software and image processing

The aerial photos collected during the flights are processed using the Agisoft Metashape Professional software (https://www.agisoft.com/). The process includes two main stages, which are block orientation and DSM generation. Since the main objective of this study is to analyse the influence of the number of GCPs on the accuracy of the DSM, all parameters of the processing are kept unchanged. Specifically, both the accuracy of photo alignment and the quality of building dense cloud were set to medium. While the former controlled the accuracy of the camera position estimation, the latter specified the desired reconstruction quality. In addition, the higher the value of the two parameters, the more accurate and comparatively detailed geometry are achieved, but it requires a substantially longer processing time. Although the level of accuracy and detail would

reduce with the setting of ‘medium’, it does not make any change on the effect of GCPs. The processing workflow is shown in Figure 3.

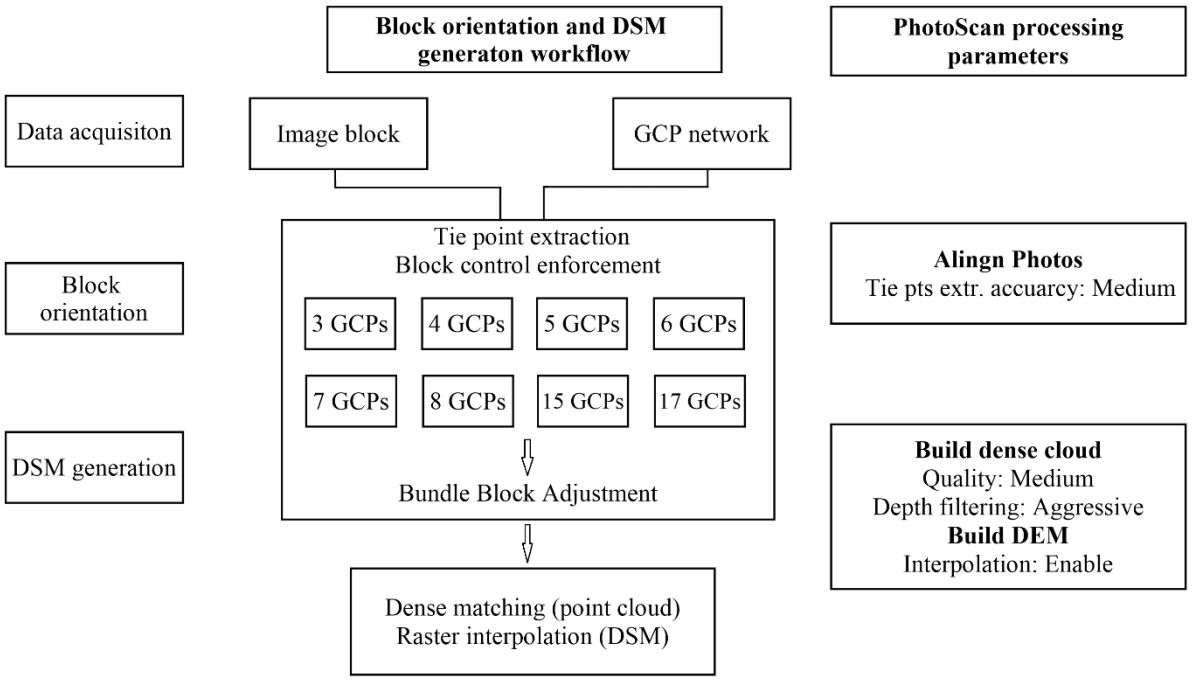

Figure 3. Data processing workflow for each case of the study by Agisoft Metashape (Forlani et al., 2018).

3.3. Accuracy assessment

The accuracy of the constructed DSMs is assessed using Root Mean Square Error (RMSE) in the horizontal ($RMSE_{XY}$) (Equation (1)), vertical ($RMSE_Z$) (Equation (2)), and overall components ($RMSE_{XYZ}$) (Equation (3)), individually for all the 40 DSMs. This is a frequently used method for assessing multiple DSMs in the literature (e.g., Agüera-Vega et al., 2017). The RMSEs for the three components are computed as:

$$RMSE_{XY} = \sqrt{\left(\frac{1}{n}\right)\sum_{i=1}^{n}\left[(\mathrm{X_{DSM}}-\mathrm{X_{GCP}}_i)^2 + (\mathrm{Y_{DSM}}-\mathrm{Y_{GCP}}_i)^2\right]} \quad (1)$$

$$RMSE_Z = \sqrt{\left(\frac{1}{n}\right)\sum_{i=1}^{n}(\mathrm{Z_{DSM}}-\mathrm{Z_{GCP}}_i)^2} \quad (2)$$

$$RMSE_{XYZ} = \sqrt{\left(\frac{1}{n}\right)\sum_{i=1}^{n}(\mathrm{X_{DSM}}-\mathrm{X_{GCP}}_i)^2 + (\mathrm{Y_{DSM}}-\mathrm{Y_{GCP}}_i)^2 + \left(\mathrm{Z_{DSM}}-\mathrm{Z_{GCP}}_i\right)^2} \quad (3)$$

where, n is the total number of check points, $(X_{GCP}, Y_{GCP}, Z_{GCP})$ and $(X_{DSM}, Y_{DSM}, Z_{DSM})$ are the 3D coordinates of a given point obtained using GNSS survey and corresponding

coordinates on the generated DSM, respectively. Hereafter, this is referred as inter-case assessment.

An intra-case assessment is also performed for all the eight cases. To observe the influence of the different configurations of the same number of GCPs on the DSM generation, i.e. the extent and variability of errors, the range of RMSEs in all the components (horizontal, vertical, and overall) for five configurations of the eight cases each are computed using equations (4-6).

$$\Delta RMSE_{XY} = RMSE_{XY\_max} - RMSE_{XY\_min} \quad (4)$$

$$\Delta RMSE_{Z} = RMSE_{Z\_max} - RMSE_{Z\_min} \quad (5)$$

$$\Delta RMSE_{XYZ} = RMSE_{XYZ\_max} - RMSE_{XYZ\_min} \quad (6)$$

4. Results and discussions

The result of the block orientation in terms of camera locations and image residuals are shown in Figures 4a and 4b, respectively. The internal and external orientation parameters of the camera are also determined that comprises 13 parameters. The definition of these 13 parameters are listed in Table 2 while Table 3 depicts their values.

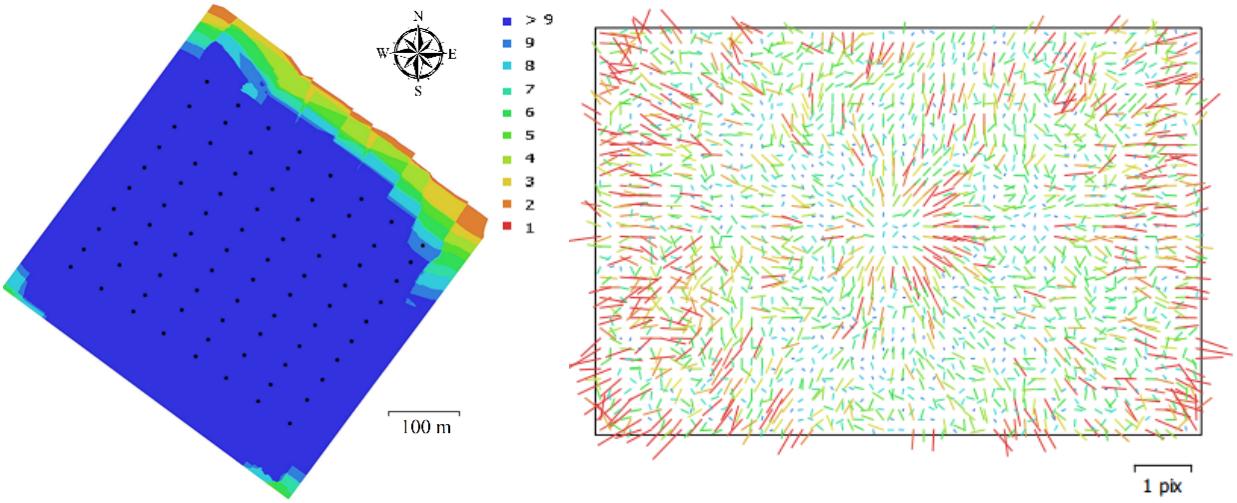

(a) (b)

Figure 4 (a) Camera locations and image overlap; (b) image residuals (for Case 2 and produced by Agisoft Metashape).

Table 2. Camera-lens parameters

No	Parameter	Explanation
1	f	Focal length (in pixels)
2	Cx, Cy	Principal point offset of the image in x and y image coordinates (in pixels)
3	B1, B2	Affinity and skew coefficients (in pixels)

4	K1, K2, K3, K4	Radial distortion coefficient of 2nd, 4th, 6th, 8th-order, respectively (dimensionless)
5	P1, P2, P3, P4	Tangential distortion coefficient (dimensionless)

Table 3. Camera-lens calibrated coefficient (for Case 2)

No	Parameter	Value	Error
1	f	3870.71	0.38
2	Cx	5.08145	0.019
3	Cy	-1.54674	0.016
4	B1	-12.6349	0.03
5	B2	-17.4018	0.026
6	K1	0.006692	0.000059
7	K2	-0.05837	0.00031
8	K3	0.119846	0.00065
9	K4	-0.08103	0.00047
10	P1	0.000889	1.4E-06
11	P2	-0.0012	9.5E-07
12	P3	0.652888	0.014
13	P4	-0.43653	0.013

The results of the accuracy assessment for cases one and two are depicted in Table 4 and Figure 5, while for all the other cases, they are depicted in Table 5 and Figure 7. The results in Figure 5 are for the configurations with minimum $RMSE_{XYZ}$ among all the five configurations for cases one and two. The results in Figure 7 are for the configurations with maximum $RMSE_{XYZ}$ among all the five configurations for cases three to eight.

Table 4. The accuracy of the model in case 1 and case 2.

Case 1: (3-15)			
Control points	$RMSE_{XY}$ (m)	$RMSE_Z$ (m)	$RMSE_{XYZ}$ (m)
8; 13; 18	0.671	1.874	1.990
8; 13; 21	0.764	2.233	2.360
9; 16; 24	0.673	1.624	1.758
9; 13; 23	0.809	2.204	2.348
12; 17; 20	0.463	1.761	1.821
Case 2: (4-14)			
Control points	$RMSE_{XY}$ (m)	$RMSE_Z$ (m)	$RMSE_{XYZ}$ (m)
8; 12; 15; 25	0.174	0.227	0.286
9; 11; 16; 23	0.234	0.390	0.455
9; 13; 16; 24	0.276	0.374	0.465
11; 14; 18; 22	0.298	0.124	0.323
12; 14; 17; 25	0.144	0.135	0.198

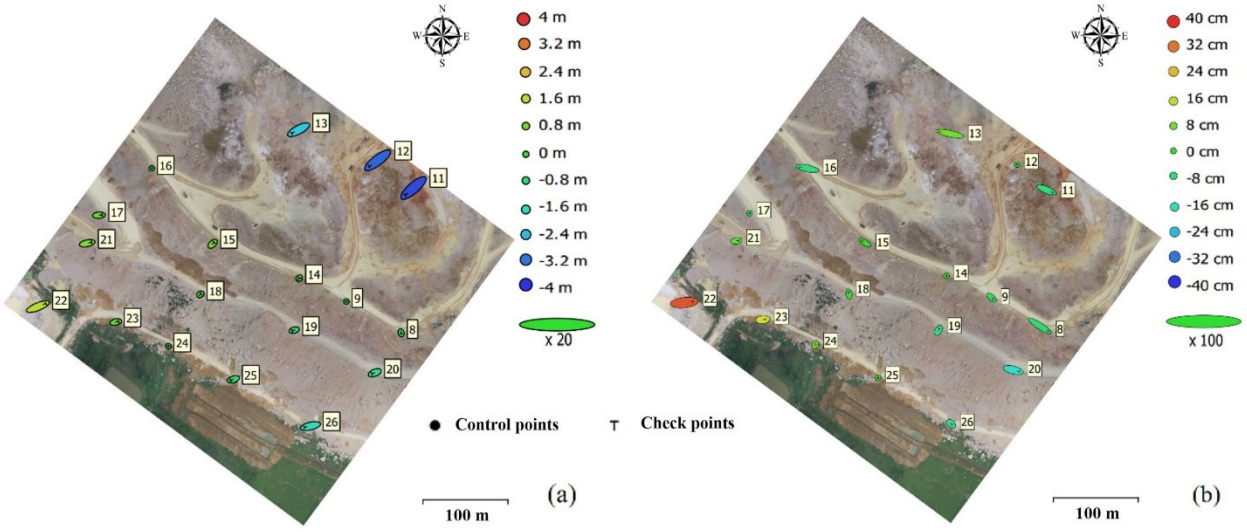

Figure 5. GCP locations and error estimates (a) – case 1 and (b) – case 2.

From Table 4, the large values of RMSEs for case 1 shows that a built model using only 3 GCPs presents a sensitively inferior DSM in terms of reliability. Moreover, the larger range values for case 1 suggest that the accuracy of a DSM is significantly dependent on the configuration if very few GCPs are used. A drop of maximum $RMSE_{XYZ}$ of 2.36 m for case 1 to a maximum $RMSE_{XYZ}$ of 0.46 m for case 2 is attributable to the addition of one more GCP for DSM construction. The dependence of errors on the configuration can be observed in Table 6, where we have provided the range of RMSEs of the five configurations in all eight cases.

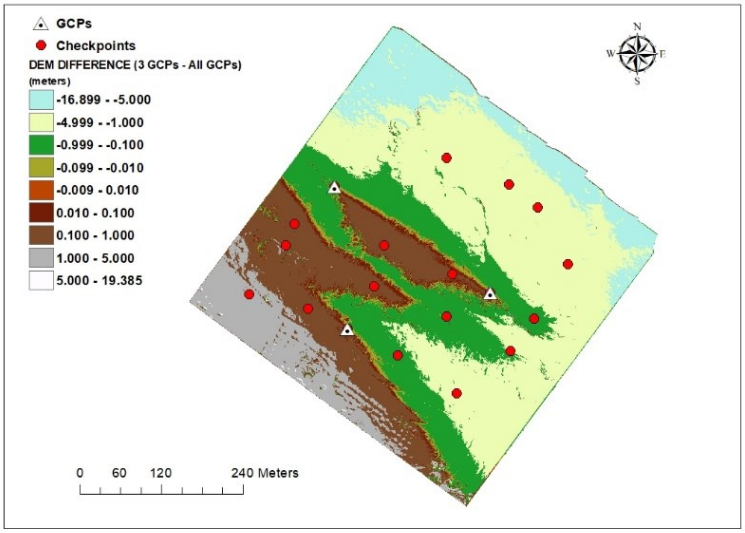

(a)

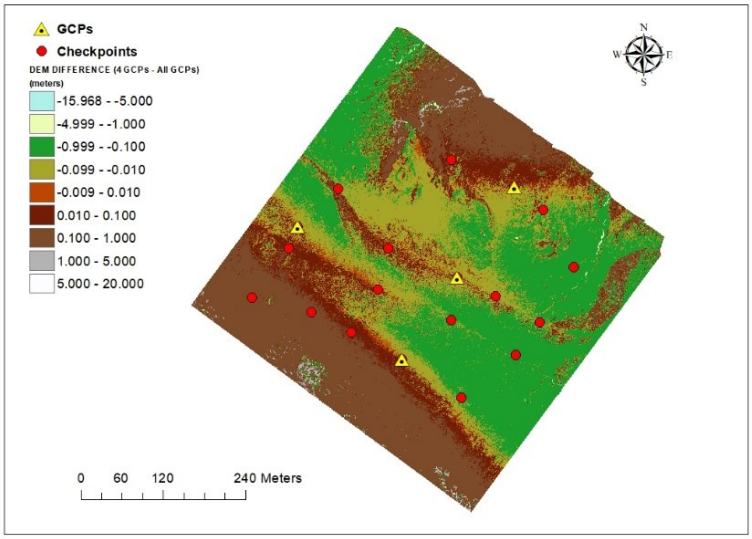

(b)

Figure 6. Differences between DSMs generated in cases of using (a) 3 GCPs; (b) 4 GCPs and all GCPs

In order to illustrate the influence of GCPs on the accuracy of DSMs, the pixel-wise difference maps were created (Figures 6a and 6b) between the pairs of DSMs from cases 1 and 2, and an ideal case using all 18 GCPs. Figures 6a and 6b suggests that the uniform distribution of the GCPs should not be done only in horizontal plane but the vertical uniformity is also required for GCPs placement. If the GCPs are only in low-lying areas, then the accuracy cannot be expected/obtained in the high-lying areas and vice-versa. Hence, vertical distribution must be strictly followed for a high-undulating terrain like open-pit mines, where we have a large range of heights. The effect of considering the vertical distribution is exemplified in figure 6a versus 6b. Furthermore, the relatively lower error in interpolation as compared to larger errors in extrapolation are also observed in both figures 6a and 6b.

Though an idea of the increase in accuracy by increasing GCPs is depicted from cases 1 and 2 in Table 4, we do not recommend the use of either three or four GCPs for DSM generation. This is because they do not meet the accuracy required for a mining project and more importantly, with the use of a fewer GCPs the DSM accuracy is highly susceptible to the different configurations of the GCPs even if they are distributed uniformly (Tables 4 and 6). Hence, DSMs generated using very few GCPs are uncertain and inconsistent.

Table 5. The accuracy of the model in cases 3, 4, 5, 6, 7, and 8.

Case 3: (5 control points and 13 check points)			
Control points	$RMSE_{XY}$ (m)	$RMSE_{Z}$ (m)	$RMSE_{XYZ}$ (m)

8-12-15-22-26	0.035	0.048	0.059
8-12-16-23-26	0.034	0.052	0.062
8-13-15-21-25	0.051	0.075	0.090
9-12-15-21-25	0.062	0.078	0.099
9-12-17-23-25	0.051	0.054	0.074
Average	0.047	0.061	0.076
Case 4: (6 control points and 12 check points)			
Control points	$RMSE_{XY}$ (m)	$RMSE_Z$ (m)	$RMSE_{XYZ}$ (m)
8-12-14-16-22-26	0.034	0.027	0.043
8-12-16-18-22-26	0.018	0.032	0.037
9-11-13-15-23-25	0.025	0.060	0.065
9-12-15-22-24-26	0.040	0.044	0.059
13-14-16-20-21-25	0.024	0.041	0.047
Average	0.028	0.040	0.050
Case 5: (7 control points and 11 check points)			
Control points	$RMSE_{XY}$ (m)	$RMSE_Z$ (m)	$RMSE_{XYZ}$ (m)
8-11-13-16-18-22-26	0.019	0.014	0.024
8-12-15-16-19-21-23	0.019	0.039	0.043
9-12-15-16-21-24-26	0.023	0.033	0.040
11-13-16-19-20-23-25	0.022	0.021	0.030
12-14-15-16-20-23-25	0.029	0.027	0.040
Average	0.022	0.026	0.035
Case 6: (8 control points and 10 check points)			
Control points	$RMSE_{XY}$ (m)	$RMSE_Z$ (m)	$RMSE_{XYZ}$ (m)
8-11-13-14-16-18-22-26	0.018	0.022	0.028
8-12-15-16-19-21-23-26	0.026	0.015	0.041
9-11-13-15-16-17-23-26	0.032	0.020	0.038
11-12-14-15-16-20-23-25	0.018	0.027	0.032
11-13-14-16-18-20-22-25	0.020	0.023	0.029
Average	0.023	0.021	0.033
Case 7: (15 control points and 3 check points)			
Checked points	$RMSE_{XY}$ (m)	$RMSE_Z$ (m)	$RMSE_{XYZ}$ (m)
9-12-18	0.013	0.009	0.016
11-15-25	0.009	0.020	0.022
13-14-26	0.019	0.024	0.031
14-17-20	0.020	0.019	0.028
16-19-23	0.022	0.026	0.034
Average	0.017	0.019	0.026
Case 8: (16 control points and 2 check points)			
Checked points	$RMSE_{XY}$ (m)	$RMSE_Z$ (m)	$RMSE_{XYZ}$ (m)
9-21	0.015	0.015	0.022
11-23	0.007	0.028	0.029
16-26	0.018	0.024	0.031

17-20	0.011	0.018	0.022
12-24	0.009	0.019	0.021
Average	0.012	0.020	0.025

From Table 5 and Table 6, the same set of observations is found for the other cases, i.e., with the GSD of images ranging from 4.66 cm/pixel to 7.58 cm/pixel the increase in the number of GCPs, i) the accuracy of a DSM improves and ii) the dependence on the configuration of GCPs decreases. The minimum $RMSE_{XYZ}$ for case 3 and case 8 are 0.059 m and 0.021 m, respectively. It is observed from Table 5 that the average $RMSE_{XY}$ and average $RMSE_Z$ are improved from 0.047 m and 0.061 m for case 3 to 0.012 m and 0.020 m for case 8, respectively. Considering Table 4 to Table 6, a drastic improvement is observed in the accuracy of a DSM when the number of GCPs increases from 3 to 4 and from 4 to 5, respectively. Comparatively less significant improvement occurred when GCPs are increased from 5 to 6 and further to 7. Although case 3 with 5 GCPs is sufficient for our purpose, a 2-cm improvement in the height accuracy is observed with 6 GCPs. So, we suggest using 6 GCPs for a DSM generation of small to medium-sized open-pit mines, with areas up to 36 hectares with some cautions on the configuration. However, as a factor of safety, 7 GCPs is highly recommended as it has sub-centimetre dependence on the network configuration, with the condition of uniform distribution.

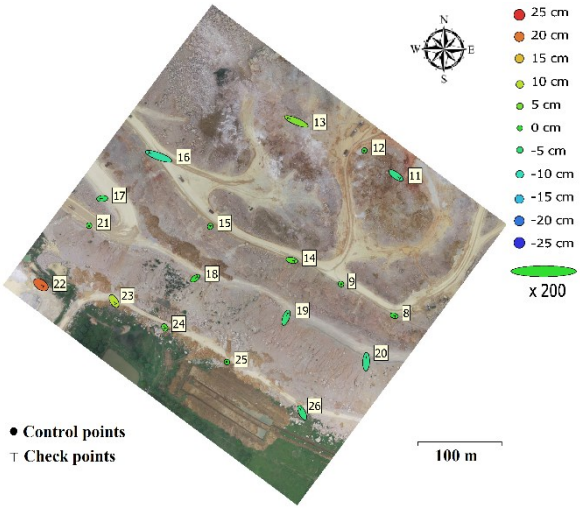

(a)

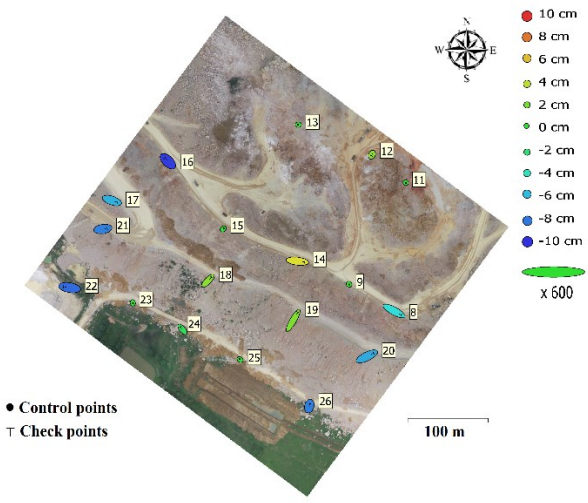

(b)

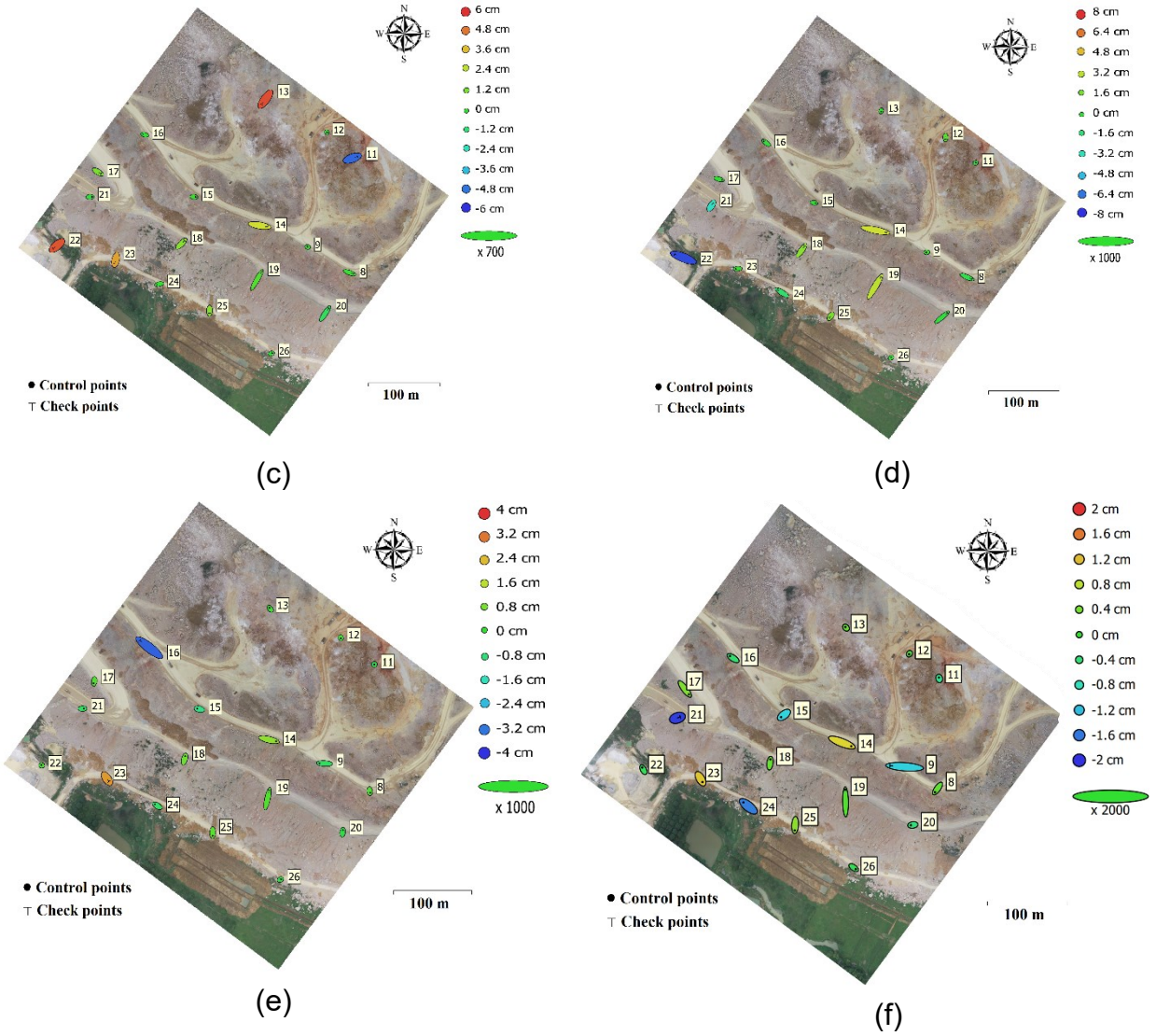

Figure 7. GCP locations and error estimates (a) case 3, (b) case 4, (c) case 5, (d) case 6, (e) case 7, and (f) case 8.

The color of the error ellipses in Figure 5 and Figure 7 indicates the error in the Z component of the GCPs, while the ellipse shape represents the error in the X and Y components. Table 6 represents differences between the max and min RMSEs in five configurations for all the eight cases hence, depicting the spread of the error for different configurations of a given number of GCPs.

Table 6. Differences between the max and min RMSEs in five configurations for all the eight cases.

Case	$\Delta RMSE_{XY}$ (m)	$\Delta RMSE_{Z}$ (m)	$\Delta RMSE_{XYZ}$ (m)
1	0.346	0.609	0.602
2	0.154	0.266	0.267
3	0.028	0.030	0.040
4	0.022	0.033	0.028
5	0.010	0.025	0.019

6	0.014	0.012	0.013
7	0.013	0.017	0.018
8	0.011	0.013	0.010

5. Conclusion

In this study, a detailed investigation has been conducted on the influence of the number of GCPs and their network configurations on the quality of DSM generated using the UAV-based method over small quarries. A lightweight DJI Phantom 4 Pro UAV was used to generate 40 DSMs of the Long Son quarry in Thanh Hoa province, Vietnam. The analysis was carried out on five configurations of each of the eight combinations of 18 GCPs for DSM generation and accuracy assessment.

It is concluded from experiments that with the increase in the number of GCPs, the accuracy of DSMs increases and the dependence on the network configuration decreases. However, a precise DSM is required at regular intervals of time in a mining project for various applications and, therefore, we tried to find an optimal solution for small to medium-sized open-pit mines. This included finding the optimal number of GCPs to obtain sufficiently accurate DSMs while maintaining safety, time, and cost effectiveness. The results showed that to achieve an average accuracy well within 10 cm, five GCPs are sufficient and six GCPs to obtain the accuracy up to 5 cm. However, we strongly recommend using seven GCPs as it provided an average overall accuracy within 3.5 cm with vertical accuracy being 2.6 cm. Moreover, with a delta RMSE of all the components within 1.8 cm, it can be concluded that using seven GCPs decreases the dependency on network configuration. However, the condition of uniform distribution of the GCPs must be maintained.

We acknowledge that the accuracy of DSM will also be dependent on the flight height of UAVs. However, it has not been involved in our analysis. With this study we tried to fill a possibly literature gap on the influence of the number of GCPs on DSM generation of the small to medium-sized open-pit mines using lightweight UAVs. Working and presenting the results from open-pit mines, UAV-based survey seems to be a valid and an efficient approach for mapping in the rugged topographies, and thus, further applications in the mining industry.

Acknowledgements

This work was financially supported by the Ministry of Education and Training (MOET) in Vietnam under grant number B2020-MDA-14.

Data Availability Statement

Some or all data, models, or codes that support the findings of this study are available from the corresponding authors upon reasonable request.

Conflicts of Interest: The authors declare no conflict of interest.

References

1. James, M.R., et al., Optimising UAV topographic surveys processed with structure-from-motion: Ground control quality, quantity and bundle adjustment. Geomorphology, 2017. 280: p. 51-66.
2. James, M.R., et al., 3-D uncertainty-based topographic change detection with structure-from-motion photogrammetry: precision maps for ground control and directly georeferenced surveys. Earth Surface Processes and Landforms, 2017. 42(12): p. 1769-1788.
3. Padró, J.-C., et al., *Monitoring opencast mine restorations using Unmanned Aerial System (UAS) imagery.* Science of the Total Environment, 2019. **657**: p. 1602-1614.
4. Raeva, P., S. Filipova, and D. Filipov, *Volume computation of a stockpile-a study case comparing GPS and UAV measurements in an open pit quarry.* International Archives of the Photogrammetry, Remote Sensing & Spatial Information Sciences, 2016. **41**.
5. Fernández-Lozano, J., et al., *New perspectives for UAV-based modelling the Roman gold mining infrastructure in NW Spain.* Minerals, 2018. **8**(11): p. 518.
6. Alvarado, M., et al., *Towards the development of a low cost airborne sensing system to monitor dust particles after blasting at open-pit mine sites.* Sensors, 2015. **15**(8): p. 19667-19687.
7. Ge, L., X. Li, and A.H.-M. Ng. *UAV for mining applications: A case study at an open-cut mine and a longwall mine in New South Wales, Australia*. in *2016 IEEE International Geoscience and Remote Sensing Symposium (IGARSS)*. 2016. IEEE.
8. Malos, J., et al., *Remote monitoring of subsurface heatings in opencut coal mines.* 2013.
9. Szentpeteri, K., T. Setiawan, and A. Ismanto, *Drones (UAVs) in mining and Exploration. An application example: Pit Mapping and Geological Modelling.* Unconventional Exploration Target & new tools in mineral and coal exploration, 2016: p. 45-49.
10. Ren, Z., et al., *Fast 3-D large-scale gravity and magnetic modeling using unstructured grids and an adaptive multilevel fast multipole method.* Journal of Geophysical Research: Solid Earth, 2017. **122**(1): p. 79-109.
11. Beretta, F., et al., *Topographic modelling using UAVs compared with traditional survey methods in mining.* REM-International Engineering Journal, 2018. **71**(3): p. 463-470.
12. Bui, D.T., et al. *Lightweight unmanned aerial vehicle and structure-from-motion photogrammetry for generating digital surface model for open-pit coal mine area and its accuracy assessment*. in *International Conference on Geo-Spatial Technologies and Earth Resources*. 2017. Springer.

13. Cryderman, C., S.B. Mah, and A. Shufletoski, *Evaluation of UAV photogrammetric accuracy for mapping and earthworks computations.* Geomatica, 2014. **68**(4): p. 309-317.
14. Esposito, G., et al., *Application of UAV photogrammetry for the multi-temporal estimation of surface extent and volumetric excavation in the Sa Pigada Bianca open-pit mine, Sardinia, Italy.* Environmental Earth Sciences, 2017. **76**(3): p. 103.
15. Forlani, G., et al., *Quality assessment of DSMs produced from UAV flights georeferenced with on-board RTK positioning.* Remote Sensing, 2018. **10**(2): p. 311.
16. Francioni, M., et al., *An integrated remote sensing-GIS approach for the analysis of an open pit in the Carrara marble district, Italy: Slope stability assessment through kinematic and numerical methods.* Computers and Geotechnics, 2015. **67**: p. 46-63.
17. Kovanič, Ľ., et al., *Surveying of Open Pit Mine Using Low-Cost Aerial Photogrammetry*, in *The Rise of Big Spatial Data*. 2017, Springer. p. 121-129.
18. Kršák, B., et al., *Use of low-cost UAV photogrammetry to analyze the accuracy of a digital elevation model in a case study.* Measurement, 2016. **91**: p. 276-287.
19. Nguyen, Q.L., et al., *An approach of mapping quarries in Vietnam using low-cost Unmanned Aerial Vehicles.* Inżynieria Mineralna, 2019. **21**.
20. Shahbazi, M., et al., *Development and evaluation of a UAV-photogrammetry system for precise 3D environmental modeling.* Sensors, 2015. **15**(11): p. 27493-27524.
21. Canh, L.V., et al., *Experimental Investigation on the Performance of DJI Phantom 4 RTK in the PPK Mode for 3D Mapping Open - Pit Mines.* Journal of the Polish Mineral Engineering Society, 2020. **1**(2): p. 65-74.
22. Hugenholtz, C., et al., *Spatial Accuracy of UAV-Derived Orthoimagery and Topography: Comparing Photogrammetric Models Processed with Direct Geo-Referencing and Ground Control Points.* Geomatica, 2016. **70**(1): p. 21-30.
23. Mian, O., et al., *Direct georeferencing on small unmanned aerial platforms for improved reliability and accuracy of mapping without the need for ground control points.* The International Archives of Photogrammetry, Remote Sensing and Spatial Information Sciences, 2015. **XL**(1/W4): p. 397-402.
24. Agüera-Vega, F., F. Carvajal-Ramírez, and P. Martínez-Carricondo, *Accuracy of digital surface models and orthophotos derived from unmanned aerial vehicle photogrammetry.* Journal of Surveying Engineering, 2017. **143**(2): p. 04016025.
25. Coveney, S. and K. Roberts, *Lightweight UAV digital elevation models and orthoimagery for environmental applications: data accuracy evaluation and potential for river flood risk modelling.* International journal of remote sensing, 2017. **38**(8-10): p. 3159-3180.
26. Mancini, F., et al., *Using unmanned aerial vehicles (UAV) for high-resolution reconstruction of topography: The structure from motion approach on coastal environments.* Remote sensing, 2013. **5**(12): p. 6880-6898.
27. Rangel, J.M.G., G.R. Gonçalves, and J.A. Pérez, *The impact of number and spatial distribution of GCPs on the positional accuracy of geospatial products derived from low-cost UASs.* International journal of remote sensing, 2018. **39**(21): p. 7154-7171.
28. Tahar, K., *An evaluation on different number of ground control points in unmanned aerial vehicle photogrammetric block.* ISPAr, 2013: p. 93-98.
29. Tonkin, T.N. and N.G. Midgley, *Ground-control networks for image based surface reconstruction: An investigation of optimum survey designs using UAV derived*

imagery and structure-from-motion photogrammetry. Remote Sensing, 2016. **8**(9): p. 786.

30. Villanueva, J. and A. Blanco, *Optimization of ground control point (GCP) configuration for unmanned aerial vehicle (UAV) survey using structure from motion (SfM).* International Archives of the Photogrammetry, Remote Sensing and Spatial Information Sciences, 2019. **42**(4/W12).